Diffusion of large molecules in porous structures

Vonk, Pieter

5. Ultrafiltration of a polymer/electrolyte mixture

Introduction

Ultrafiltration is a membrane process that separates solutes by differences in size and shape. The feed is a liquid containing large molecules, such as proteins. A pressure difference forces part of the feed (the 'permeate') through the membrane. The pores in the membrane are roughly the same size as those of the molecules to be separated. So these are rejected by the membrane and kept in the 'retentate'. Ultrafiltration has found wide application in biotechnology and in related industries (Cheryan 1986). However, the details of the process are not as clear as chemical engineers would like them to be. A good mathematical description of the process would be very useful for design purposes and economic evaluations (Rajagopalan and Cheryan 1991).

Several models have been used to describe ultrafiltration. Van den Berg and Smolders (1989) and Van Oers et al. (1992) have applied Fick's law in the boundary layer to calculate the fluxes in dead-end ultrafiltration. Holeschovsky and Cooney (1991) have used this approach in a continuous, rotating ultrafiltration device. Jonsson (1985) has used Fick's law inside the membrane to calculate the rejection coefficient of a solute. He calculated the effective diffusivity in the membrane using the Ferry-Faxén equations (Faxén 1923, Ferry 1936 and Renkin 1954). The Ferry equation describes geometrical exclusion of spherical macromolecules from cylindrical pores. The Faxén equation estimates the hydrodynamic friction of the solutes once they have entered the pores. It assumes that the spheres follow the centerline of the pores. This idea has been extended by Anderson and Quinn (1974) and Bungay and Brenner (1973) to calculate the influence of diffusion and convection on the process of ultrafiltration. Other hydrodynamic models are given by Deen (1987). Sahimi and Jue (1989) apply these models to a cubic network of pores with different sizes.

Irreversible thermodynamics has been used mainly in the formulation developed by Kedem and Katchalsky (1958). Slezak and Turczynski (1986) and Slezak (1989) have used this description for measurements

where gravitational effects play an important role. Tsuru et al (1990) have incorporated charge effects.

The Maxwell-Stefan equations have also been used by several authors. Pham et al (1985) used these equations to describe reverse osmosis membranes. Robertson and Zydney (1988) used a combination of Fick's law in the boundary layer and the Maxwell-Stefan equation in the membrane to describe dead-end ultrafiltration. They did not include viscous flow in their model. Thiel and Lloyd (1988) derived a matrix equation for a dilute solution assuming constant component properties.

Several features of the Maxwell-Stefan equations can be found in the models given above. We have explored others, including:

- multiple driving forces: activity, electrical and pressure gradients,
- multiple resistances from boundary layers, fouling layers and the membrane,
- the effects of thermodynamic non-ideality of the solutions,
- charge effects and effects of added electrolytes and
- the effect of viscous or convective flow through the membrane.

For this purpose, we need a fairly general form of the Maxwell-Stefan equations.

Developing a model of ultrafiltration

An ultrafiltration module consists of an upstream or concentrate compartment, and a downstream or permeate compartment. These are separated by the membrane. (Figure 5.1). The upstream compartment is turbulent and well mixed by a liquid recycle. We also assume that the permeate has the same composition everywhere. A pressure difference forces the permeate through the membrane. This causes an accumulation of the rejected molecules in the boundary or 'polarization' layer before the membrane. Accumulation rapidly reaches a steady state, where transport by convection into the boundary layer is balanced by diffusion back into the bulk of the liquid. So the elements of our model are:

- a well-mixed bulk fluid upstream,
- a boundary layer,
- the membrane and
- a well-mixed downstream compartment.

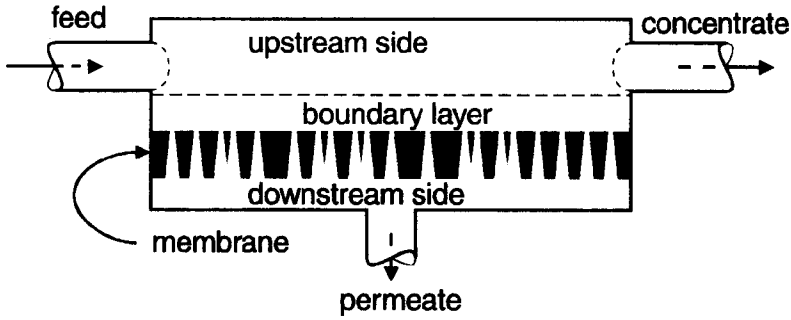

Figure 5.1 : A single ultrafiltration stage

To describe these elements we need four different kinds of relations:

- mass balances,
- transport relations,
- equilibrium relations and
- constraint relations.

These relations have to be solved for the membrane and the boundary layer and coupled to the conditions in the bulk fluids.

Mass balances

The model simulates steady state mass transfer. It contains no accumulation terms, so the balance equations simply state that the molar fluxes through the boundary layer must equal the fluxes through the membrane:

$$N_i^b = N_i^m \tag{5.1}$$

In addition, the ratio of two molar fluxes is equal to that of the mole fractions in the permeate because no resistance is situated at the back-end of the membrane:

$$\frac{N_i}{N_j} = \left.\frac{x_i}{x_j}\right|_{permeate} \tag{5.2}$$

Transport relations in the membrane

Diffusional transport is governed by the Maxwell-Stefan equations. The relations for the liquid in the boundary layer are no different from those discussed earlier, but in the membrane there are complications. The membrane itself is an extra component, and we must also reckon with convective flow through the pores.

We take the membrane to consist of an inert polymer matrix with pores. We first consider diffusion of small species such as water and ions. The diffusing species and the membrane exert friction on each other, but otherwise diffusion occurs in the same way as in free solution. Because the membrane does not have a well-defined mole fraction, we add friction with the membrane as a separate term:

$$\left(-\nabla_p \mu_i - Fz_i \nabla\phi - v_i \nabla p\right)_{in\ pores} = \sum_j \frac{RT}{\mathcal{D}_{ij}^o} x_j \left(u_i - u_j\right)_{in\ pores} + \frac{RT}{\mathcal{D}_{im}^o}\left(u_i - u_m\right)_{in\ pores} \tag{5.3}$$

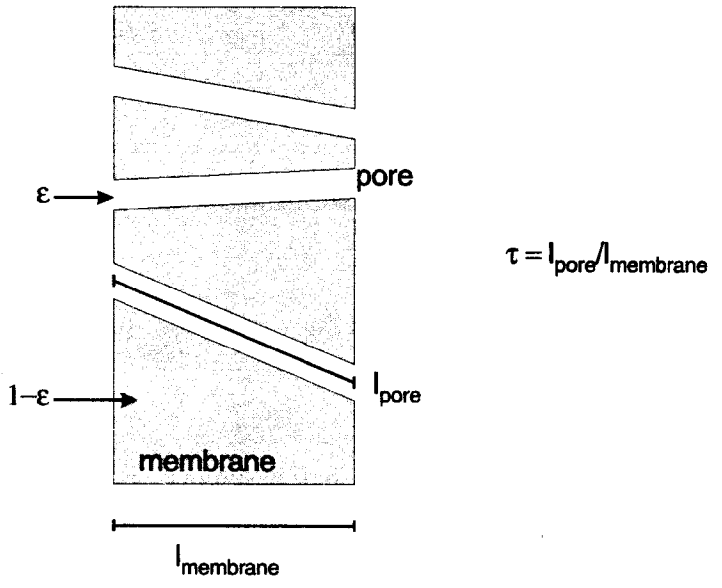

Figure 5.2: The membrane model.

Gradients, compositions and velocities in this equation are values in the pores. The velocity u_m of the membrane is zero, of course: we have only retained it to show the structure of the equation. Diffusivities D_{ij}^o are the values in free solution.

The pores do not pass straight through the membrane; it is instructive to consider them as cylinders, at an angle to the membrane surface (Figure 5.2). The length of the pores is τ times the membrane thickness; τ is the 'tortuosity'. This has two effects:

- It increases the length of the diffusion path and reduces the gradient by a factor τ.
- Also, it increases the diffusion velocity for a given flux, again by a factor of τ.

The area available for diffusion is smaller than the membrane area by a factor of ε. (For simple geometries, ε is also the void fraction of the membrane). For a given flux, this increases the velocities by a factor $1/\varepsilon$. The transport equation becomes:

$$-\frac{1}{\tau}\left(\nabla_p \mu_i + Fz_i \nabla\phi + v_i \nabla p\right) = \sum_j \frac{\tau}{\varepsilon}\frac{RT}{D_{ij}^0} x_j \left(u_i - u_j\right) + \frac{\tau}{\varepsilon}\frac{RT}{D_{im}^0}\left(u_i - u_m\right) \tag{5.4}$$

Here the gradients and velocities are perpendicular to the membrane. We can rewrite this as:

$$-\nabla_p \mu_i - Fz_i \nabla\phi - v_i \nabla p = \sum_j \frac{RT}{D_{ij}} x_j \left(u_i - u_j\right) + \frac{RT}{D_{im}}\left(u_i - u_m\right) \tag{5.5}$$

The ij diffusivities are related to those in free solution via:

$$D_{ij} = \frac{\varepsilon}{\tau^2} D_{ij}^o \tag{5.6}$$

For the *im* diffusivities, we will need to make further assumptions, or to obtain these from our experiments.

Our pores are sufficiently large, that convective (viscous) flow through them is important. The viscous flow velocity follows from Darcy's law:

$$w = -\frac{B}{\eta}\nabla p = -\frac{d_p^2 \varepsilon}{32\eta\tau^2}\nabla p = -\frac{B_o \varepsilon}{\eta\tau^2}\nabla p \tag{5.7}$$

B is the permeability of the membrane. In a mixture, the viscous flow velocity need not be the same for all components. For example, large molecules may stay in the middle of the pores, so that they have a velocity higher than average. However, we do not take this into account.

Diffusion and convection are simultaneous parallel processes; they give a net species velocity:

$$v_i = u_i + w \tag{5.8}$$

Combining equations 5.5, 5.7 and 5.8 yields:

$$-\nabla_p \mu_i - Fz_i \nabla\phi - \left(v_i + \frac{RTB}{\eta \mathcal{D}_{im}}\right)\nabla p = \sum_j \frac{RT}{\mathcal{D}_{ij}} x_j (v_i - v_j) + \frac{RT}{\mathcal{D}_{im}}(v_i - v_m) \tag{5.9}$$

This is a special case of a general equation that Mason and Lonsdale (1990) have derived, based on statistical mechanics. The difference is, that we take the convective velocities of all species to be equal. We can also write the equation in terms of fluxes:

$$N_i = v_i c_i = v_i x_i c_{tot} \tag{5.10}$$

$$-\frac{x_i}{RT}\nabla_p \mu_i - \frac{x_i z_i F}{RT}\nabla\phi - x_i\left(\frac{v_i}{RT} + \frac{B}{\mathcal{D}_{im}\eta}\right)\nabla p = \sum_j \frac{x_j N_i - x_i N_j}{c_{tot}\mathcal{D}_{ij}} + \frac{N_i}{c_{tot}\mathcal{D}_{im}} \tag{5.11}$$

This is the working equation that we will use in the rest of this chapter.

Transport in the boundary layer

The bulk of the fluid in the upstream compartment, is rapidly mixed by turbulence. However, near the membrane boundary, turbulence dies out and transport to the membrane is taken over by diffusion and drift. We assume that this happens at a certain distance δ' from the membrane. In binary mass transfer, the thickness of the boundary layer is often described as a relation between dimensionless numbers. For a geometry of the type considered here, the relation might be:

$$Sh = Const \cdot Re^{0.8} \cdot Sc^{0.33} \quad \text{or} \quad \frac{\delta'}{d'} = Const \cdot \left(\frac{\rho v d'}{\eta}\right)^{0.8} \left(\frac{\nu}{\mathcal{D}}\right)^{0.33} \tag{5.12}$$

For a multicomponent solution with different $\mathcal{D}$'s, this leads to different values of the boundary layer thickness for different components. To avoid this, we have neglected the weak effect of the Schmidt number by using the Schmidt number of water/PEG-4000 in all the calculations. We obtain the 'constant' from the effect of the fluid velocity v in our experiments.

Equilibrium and constraint relations

Besides the mass balance and the MS-equations (one for each component in both the membrane and the boundary layer), we also need equilibrium and constraint relations to describe the ultrafiltration module. The constraint relations state that the mole fractions add up to one and that the solution is electrically neutral:

$$\sum_j x_j = 1 \tag{5.13}$$

$$\sum_j x_j z_j = 0 \tag{5.14}$$

Even at equilibrium, the concentration of solutes in the pores is not equal to the concentration in free solution. Large molecules will be partly

excluded from the membrane if their diameter approaches that of the pores (Figure 5.3). Ions will be attracted by a matrix with an opposite electrical charge, but repelled by a like charge. These concentration differences cause a jump in electrical potential and pressure at the membrane/liquid interface. We describe the resulting equilibria with:

$$RT \ln\left(\gamma_i^{steric}\gamma_i^{y} y_i\right) + Fz_i\phi' + v_i p' = RT \ln\left(\gamma_i^{x} x_i\right) + Fz_i\phi + v_i p \quad (5.15)$$

or

$$\frac{y_i}{x_i} = K\frac{\gamma_i^{x}}{\gamma_i^{y}} \exp\left(-\frac{Fz_i\Delta\phi}{RT}\right)\exp\left(-\frac{v_i\Delta p}{RT}\right) \quad (5.16)$$

We obtain the activity coefficients γ_i and γ_i' from the relations derived in the previous chapter. The two values differ because the composition of the liquid in the pores differs from that in the boundary layer. The coefficient K allows for other differences between pore and bulk liquid; these are mainly due to steric exclusion. This effect is especially important for large molecules, in our case for PEG.

The electrical potential difference $\phi - \phi'$ between the external and pore liquid is mainly caused by charges in the membrane material. This charge causes exclusion of ions from the pores for low electrolyte concentrations; we find its value from this effect on our experiments.

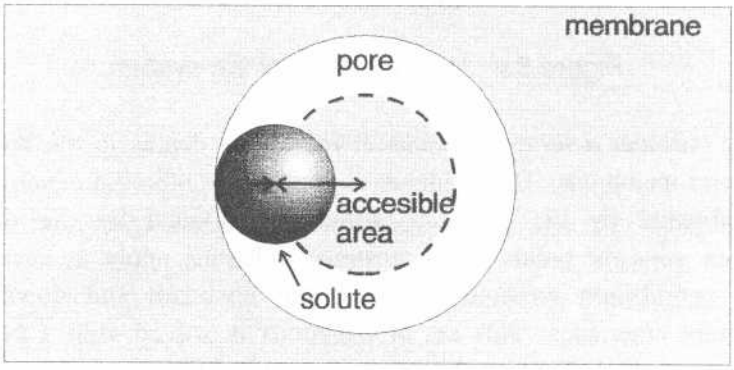

Figure 5.3 : The steric exclusion mechanism in a cylindrical pore.

Numerical method

The model yields a set of nonlinear ordinary differential equations with boundary conditions at different spots. These probably do not have analytical solutions, so we have solved them numerically. Two methods exist to solve our type of equations: the shooting and the relaxation method. The former is not a good method to use here, because of the coexistence of the boundary layer and the membrane, which causes sharp gradients and large non-linearities (Figure 5.4). So we solve the equations with a relaxation method.

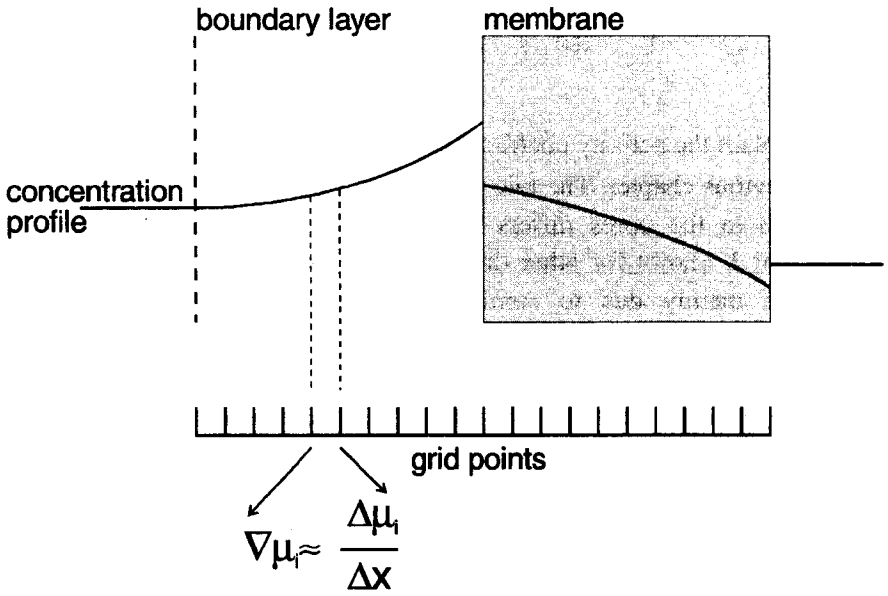

Figure 5.4 : Discretisation of the system.

We consider a series of points at increasing depths in the boundary layer and membrane. The gradients in the Maxwell-Stefan equations are approximated by the potential differences divided by the distance between adjacent points. The constraint relations apply at each point while equilibrium relations apply at the upstream and downstream membrane interfaces. This set of equations is solved with a Newton-Raphson method. This results in a sparse Jacobi matrix, so we do not need to save all the elements of the matrix. The mole fractions, electrical potential and pressure derivatives in the matrix are grouped according to the numbering of the grid points. The mole flux derivatives are put at the

right-hand side of the matrix. Only the central diagonal, the first lower diagonal and the last column need to be saved. This matrix is easily solved by Gauss-Jordan elimination.

Ultrafiltration experiments

We have used a series of experiments with a flat membrane module to check some properties of our model. The equipment (Figure 5.5) consisted of a FILTRON Minisette system fitted with coated polysulfone ('alpha') membranes with a 3000-Dalton cutoff. The membrane cassette contained ten membranes with a total area of 0.070 m^2, placed at 0.4 mm distance. The top layer of the membrane was about 0.9 μm thick (as estimated from a microscopic picture of a non coated 'omega' membrane given to us by FILTRON). The rectangular channel between two membranes was 9 cm wide. It was fitted with a spacer to promote liquid mixing in the channel and to reduce concentration polarisation.

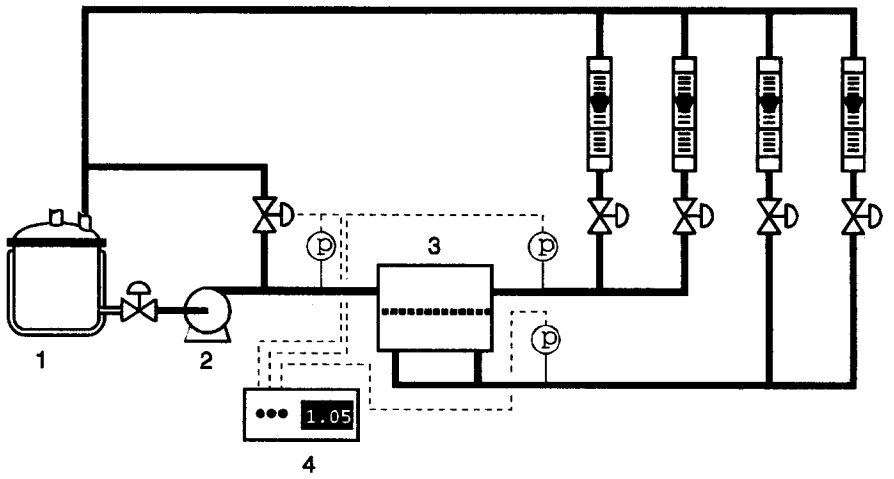

1: storage vessel
2: pump
3: membrane module
4: pressure read out

Figure 5.5 : The experimental set-up.

The storage vessel (5 litres) was kept at 25 °C by of a PMT Tamson T-1000 water bath. A Watson-Marlow gear pump transported the liquid through the membrane module. Transducers mounted at the inlet and both

outlets of the module measured the pressures. Five valves, manually operated, controlled the flows and pressures in the system. Concentration and flow measurements were done by sampling from the tubes returning the liquid to the storage vessel. During the experiments the flow rate of the feed had one of four different values (5.0, 8.4, 11.7 or 15.2 ml/s). The concentrations in the feed, the concentrate and the permeate were measured for different values of the transmembrane pressure.

We have performed experiments with liquids of increasing complexity:

- pure water,
- solutions of polyethylene glycol (PEG),
- potassium phosphate solutions and
- mixtures of PEG and phosphate.

The PEG solutions contained 0.1, 1.0 and 5.0 % mass of PEG 4000. In the solutions with phosphate, the ratio of mono- and di-hydrogen phosphate was chosen such that the pH was equal to 6.9. Concentrations of 5, 10, 25 and 50 mmol/l were applied. Experiments with mixtures of PEG and phosphate were done using 0.1 % PEG with 50 mM phosphate, 5 % PEG with 5 mM phosphate and 5 % PEG with 50 mM phosphate.

PEG-4000 from the single solute experiments was analysed by a spectroscopic method (Crabb and Persinger 1964). PEG-4000 from the mixed solute experiments was measured by gel permeation chromatography. The analysis was done with the gel permeation chromatograph used in Chapter 2, but with a Waters refractometer instead of the UV-1 detector. The gel used was Sephadex G-25. The elution fluid contained 1 mol/l of sodium chloride to suppress ionic interaction of potassium phosphate with the gel.

The single solute experiments with potassium phosphate were analysed in two different ways. Initially a spectroscopic method was used, but later conductivity measurements were found to be sufficient. The phosphate concentration in the mixed solute experiments was also measured by means of the conductivity. The conductivity measurements were corrected for the amount of PEG-4000 present in the samples.

Experiments with water

With water, the flux through the membrane rises linearly with the pressure difference. The fluxes in the clean membrane are identical to those obtained with dilute phosphate solutions (Figure 5.6). Once PEG-4000 is passed through the membrane, an irreversible decrease in permeability is noticed, which does not change in time. By a more drastic cleaning procedure, soaking the membrane in a 0.1 M NaOH solution for at least half an hour, the membrane permeability is restored, but not completely. The rest of the experiments reported here have been done with a membrane which has been in contact with a PEG solution. The clean water flux of these membranes is assumed to be that of the lowest line in Figure 5.6.

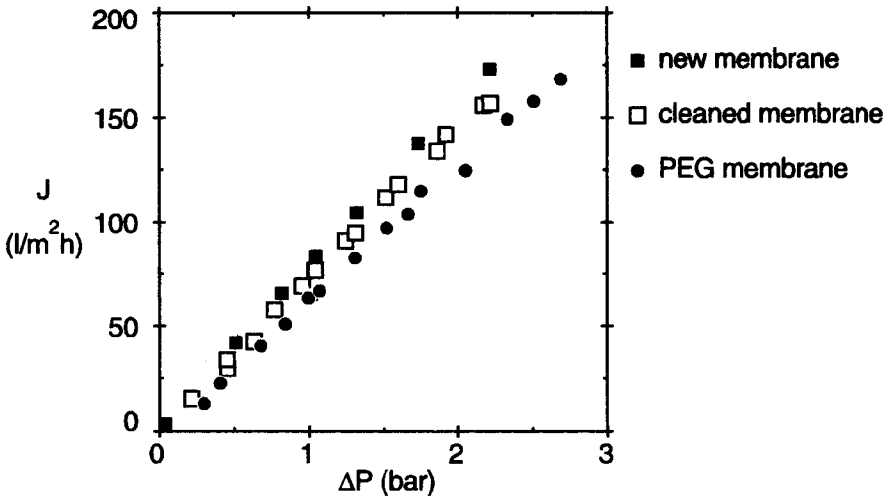

Figure 5.6: The pure water flux.

Single solute experiments of PEG-4000

The rejections of PEG-4000 at different conditions are given in Figures 5.7, while the fluxes are given in Figure 5.8. The rejection of PEG-4000 is zero when no pressure difference is applied. It rises to a maximum value and then decreases to zero with increasing pressure. The maximum is caused by several counteracting effects. With a small pressure difference, diffusion is fast enough to level out concentration differences across the membrane and the rejection goes to zero.

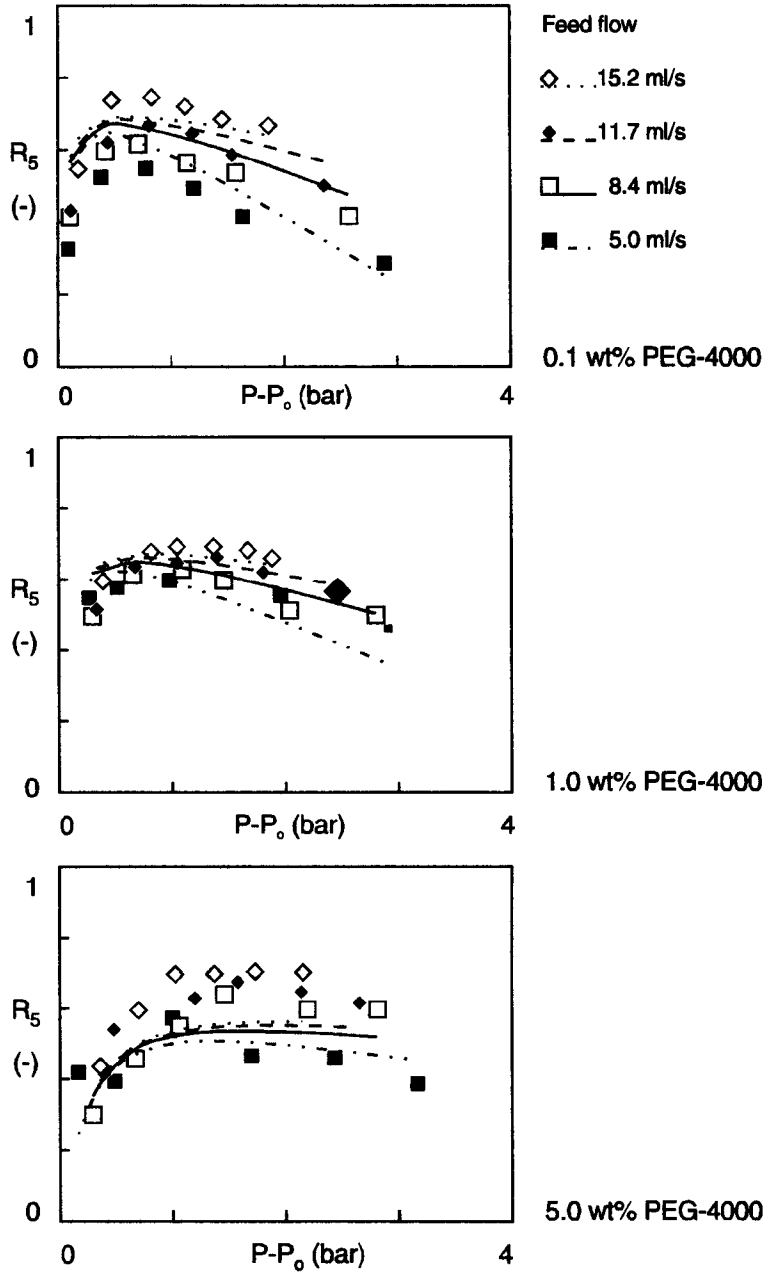

Figure 5.7 : The rejection of PEG-4000 for different concentrations (the lines represent the model).

With a higher pressure difference the membrane does reject PEG, mainly because of steric exclusion. High pressure differences and the associated fluxes, cause a strong increase of the PEG concentration next to the membrane. This then reduces the apparent rejection of the membrane. The fluxes decrease considerably with higher PEG concentrations. This decrease is much larger than would be expected from the increase of viscosity due to the PEG.

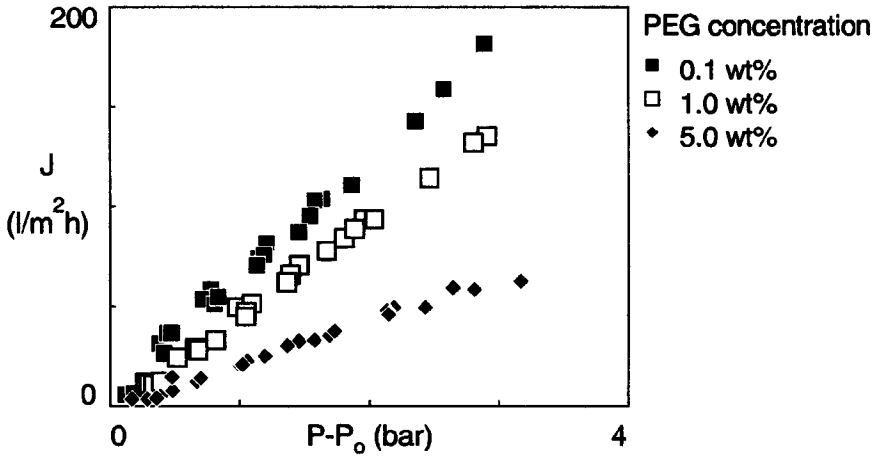

Figure 5.8 : The permeate flux for different concentrations of PEG-4000.

Single solute experiments with potassium phosphate

The rejections of potassium phosphate at different conditions are given in Figure 5.9, while the fluxes are given in Figure 5.10. The rejection of phosphate shows a strong dependence on concentration, being much higher at low concentrations. This is caused by a weak (probably negative) electrical charge of the membrane. This charge causes Donnan exclusion of the co-ions. The effect is much reduced when the phosphate concentration exceeds the charge density of the membrane. For low phosphate concentrations (where the membrane shows an appreciable rejection), the apparent rejection also depends on the velocity of the flow past the membrane. The apparent rejection increases because polarization effects then become less important. The fluxes decrease with increasing

concentration, but the effect is small. This is primarily due to increasing osmotic pressure differences across the membrane.

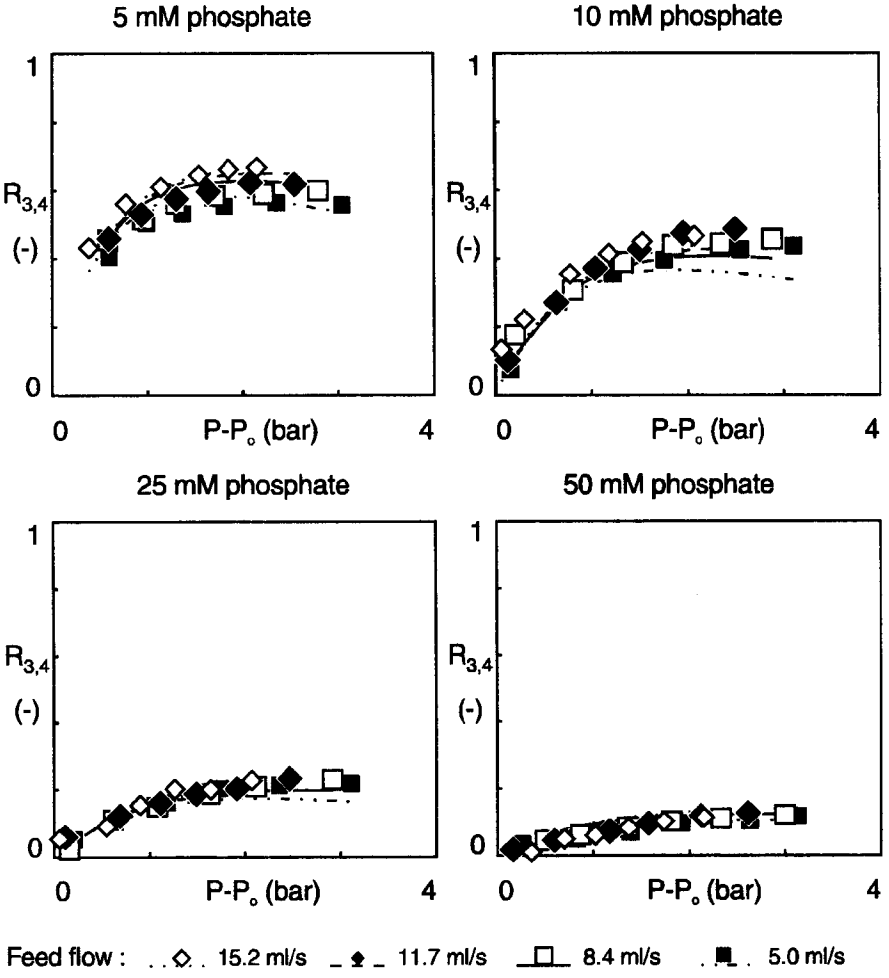

Figure 5.9 : The rejection of potassium phosphate at different concentrations (the lines represent the model).

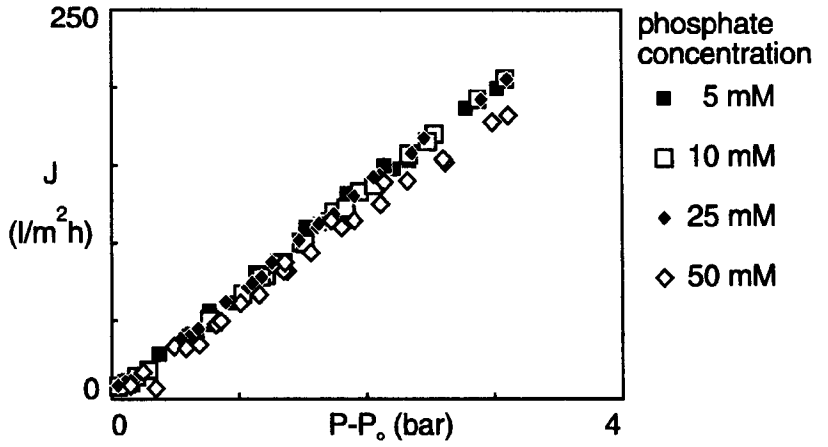

Figure 5.10 : The permeate flux at different concentrations of potassium phosphate.

Mixed solute experiments

Figure 5.11 gives the rejection coefficients of the mixed solute experiments for the different compositions. The fluxes are given in Figure 5.12. For a low pressure drop, the rejection of phosphate can be negative. Clearly phosphate is 'pushed' into the membrane by a high concentration of PEG.

Figure 5.13 gives the rejection coefficient of PEG with a 5 wt% PEG-4000 solution in the presence of different concentrations of phosphate. The results are given as a function of the permeate fluxes. Initially, the PEG rejection increases with increasing phosphate concentrations. However, further increasing the phosphate concentration from 5 mM to 50 mM phosphate decreases the rejection. To obtain the same flux at higher phosphate concentrations, a larger pressure difference is required. This increases the driving force on PEG and reduces its rejection. Figure 5.14 gives the rejection coefficient of 5 mM potassium phosphate in the presence of different concentrations of PEG-4000. The rejection of phosphate decreases in the presence of PEG-4000.

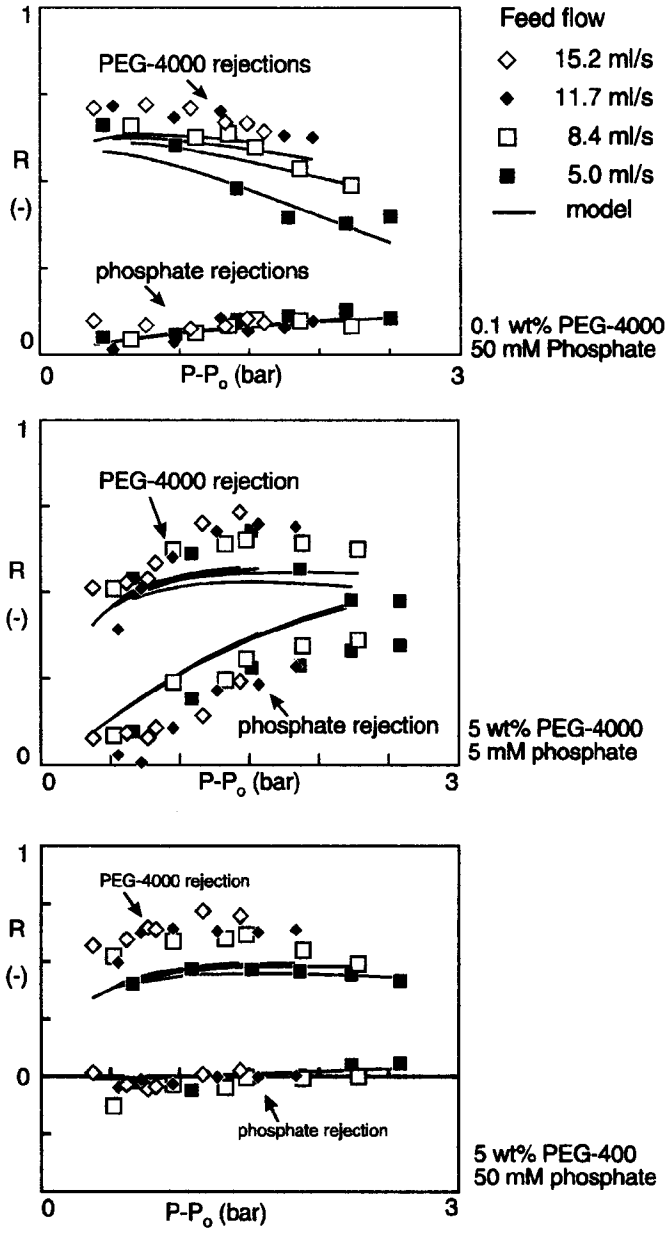

Figure 5.11 : The rejection of the mixed solute ultrafiltration experiments.

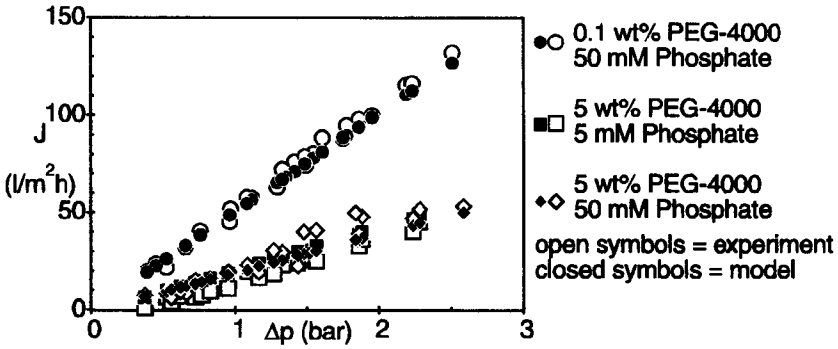

Figure 5.12 : The fluxes of the mixed solute experiments.

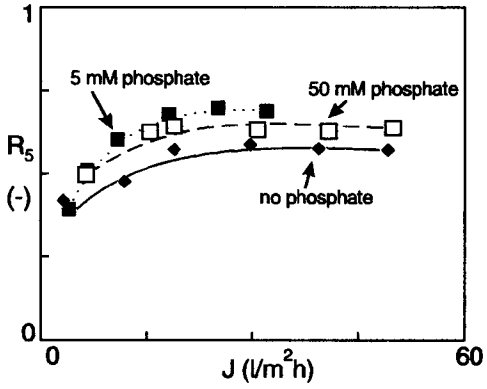

Figure 5.13 : The rejection of PEG-4000 (5 wt% PEG-4000) at different potassium phosphate concentrations.

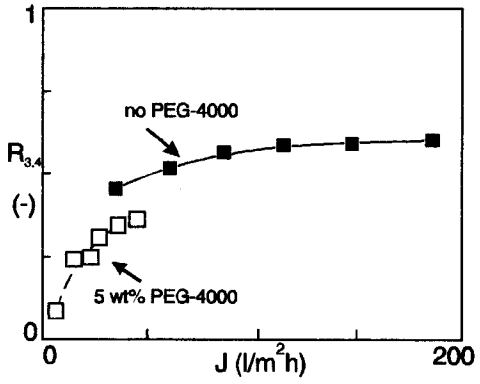

Figure 5.14 : The rejection of potassium phosphate (5 mM phosphate) at different PEG-4000 concentrations.

Model Parameters

The model contains six components: water (1), PEG (2), K^+ (3), $H_2PO_4^-$ (4), HPO_4^{2-} (5) and the membrane (6). Of these, we need a large number of properties, both for the pure components and for their interactions. In addition we need a number of geometrical parameters to describe the membrane and the boundary layer.

To describe the equilibria at the membrane/liquid interface, we need five pairs of activity coefficients, five distribution coefficients, charge numbers and molar volumes:

γ_1	γ_2	γ_3	γ_4	γ_5
γ_1'	γ_2'	γ_3'	γ_4'	γ_5'
K_1	K_2	K_3	K_4	K_5
(z_1)	(z_2)	z_3	z_4	z_5
v_1	v_2	v_3	v_4	v_5

In addition we need the charge concentration C in the membrane.

For the liquids, we need the density ρ and viscosity η. We also need a large number of diffusivities to describe interactions between species:

in the membrane

D_{12}	D_{13}	D_{14}	D_{15}	D_{16}
	D_{23}	D_{24}	D_{25}	D_{26}
		D_{34}	D_{35}	D_{36}
			D_{45}	D_{46}
				D_{56}

in the boundary layer

D_{12}'	D_{13}'	D_{14}'	D_{15}'
	D_{23}'	D_{24}'	D_{25}'
		D_{34}'	D_{35}'
			D_{45}'

Then we need a number of geometrical parameters:

- the membrane thickness δ,

- the diameter d of the pores,
- the void fraction ε,
- the tortuosity τ and
- the thickness of the boundary layer δ'.

Source of the parameters

The charge numbers and molar volumes are given in the previous chapter. We obtain the activity coefficients in the free liquid and in the pore liquid, also from the relations given there. The charge number of the membrane is set equal to minus one (because of the polysulfone membrane), and we assume that steric exclusion is negligible for water. The exclusion coefficients K_i of potassium, both phosphate ions and PEG-4000 are calculated by means of the partition theory of Ferry (1936):

$$K_i = \left(1 - \frac{r_i}{\frac{1}{2}d_p}\right)^2 = (1 - \lambda_i)^2 \tag{5.17}$$

We assume that the partial molar volume of the components is independent of composition, so the density of the solution is given by:

$$\rho = \frac{\sum_i x_i M_i}{\sum_i x_i v_i} \tag{5.18}$$

The viscosity of the solution is calculated from:

$$\ln \eta = \sum_i A_i x_i \tag{5.19}$$

The coefficients A of this equation are obtained from viscosity data. The viscosities of water/potassium phosphate-mixtures are given by Weast (1984) and the viscosity of water/PEG-400-mixtures are measured with a Ubelohde viscosity meter. The coefficients A are given in Table 5.1.

We obtain the diffusion coefficients of the solutes in water from literature (Leist 1985 and Chew and Couper 1973). They are given in Table 5.1. The diffusive ion-ion interactions are calculated by (Wesselingh and Krishna 1990):

$$Đ_{+-} = 4.8*10^{8} Đ_{I+} Đ_{I-} \frac{i^{0.55}}{|z_+ z_-|^{1.85}} \tag{5.20}$$

where

$$i = \frac{1}{2} \sum_j z_j^2 x_j \tag{5.21}$$

i (-)	component (-)	A_i (-)	$Đ_{Ii}$ (10^{-9} m^2/s)
1	H_2O	-7.024	2.0
2	K^+	79.36	1.957
3	$H_2PO_4^-$	79.36	0.860
4	HPO_4^{2-}	61.32	0.800
5	PEG-4000	1226	0.115

Table 5.1 : The viscosity and diffusion data.

The diffusive interaction between PEG and the ions is set to 10^{-10} m^2/s. This parameter (when set to a reasonable value) does not influence the outcome of the model. The water/membrane diffusion coefficient is set equal to the self-diffusion coefficient of water. Transport of water through the membrane is mainly due to viscous flow, so the exact value of this diffusion coefficient is not important.

The solute/membrane diffusion coefficients can be calculated by solving the Navier-Stokes equation in a pore in the presence of a spherical particle. The viscous interaction between the wall of the pore and the particle has two effects. An additional pressure drop is created in the pore which adds to the pressure drop across the empty pore and the friction between the sphere and its surroundings rises (enhanced drag).

The enhanced drag has been calculated by Bungay and Brenner (1973) when the sphere moves on the centerline of the pore. They calculate the force on the sphere from a diffusive and an viscous term:

$$F_s = -6\pi\eta_{water} r_s K(u_s - Gu_{water}) \tag{5.22}$$

Here K is an inverse drag coefficient and G a lag coefficient. Both depend on the ratio λ of sphere diameter to pore diameter. The subscripts s and w refer to spheres and water respectively.

We consider the friction on one mole of spheres and rewrite the equation in terms of velocity differences:

$$N_A F_s = -N_A 6\pi\eta r_s KG(u_s - u_w) - N_A 6\pi\eta r_s K(1-G)(u_s - u_m) \tag{5.23}$$

where $u_m = 0$. On the right hand side we now recognize the friction factors:

$$\frac{x_w RT}{D_{sw}} = 6\pi\eta r_s N_A KG \tag{5.24}$$

$$\frac{RT}{D_{sm}} = 6\pi\eta r_s N_A K(1-G) \tag{5.25}$$

With $x_w \to 1$ and using the Einstein-Stokes equation for diffusivity of the spheres in free solution:

$$D^o_{sw} = \frac{RT}{6\pi\eta r_s N_A} \tag{5.26}$$

we obtain:

$$\frac{D_{i,w}}{D^o_{i,w}} = \frac{1}{KG} \tag{5.27}$$

$$\frac{D_{i,m}}{D^o_{i,w}} = \frac{1}{K(1-G)} \tag{5.28}$$

The formulae for K and G are given in appendix 5. Figure 5.15 gives the diffusion coefficient calculated with equations 5.27 and 5.28. Figure 5.15 also gives the results of Computational Fluid Dynamics (CFD) simulations of the flow of a liquid through a pore containing a spherical particle (Hartholt et al 1993).

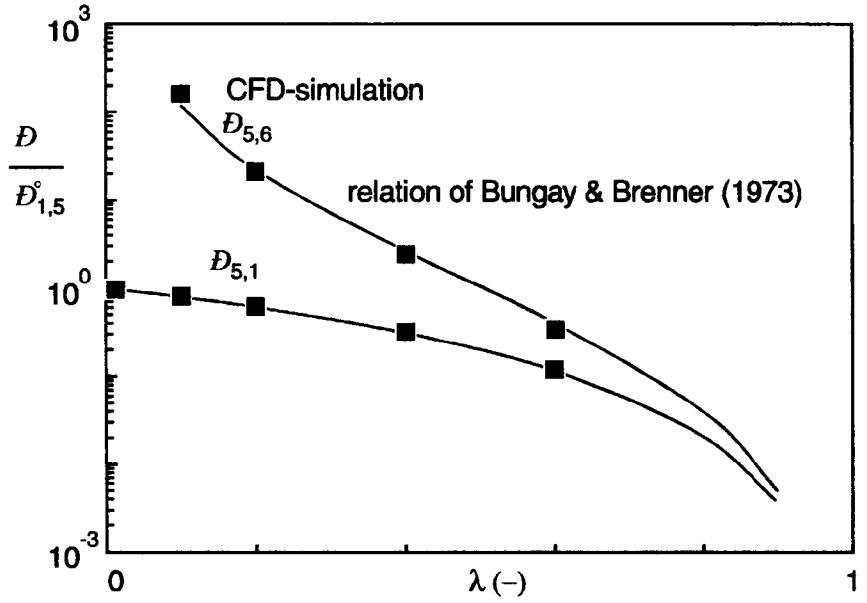

Figure 5.15 : The solute/solvent diffusion coefficient estimated from CFD-simulations and the relations of Bungay and Brenner (1973).

The CFD calculations were performed to find the pressure profiles inside the pore. Figure 5.16 gives the pressure profiles for different values of λ (the sphere and the liquid move with the same velocity). An additional pressure drop can be seen at the position of the sphere (z = 0.15). This additional pressure drop can be up to 5 % of the total pressure drop in this part of the pore. The sphere occupies a volume fraction of 0.006 in this part of the pore (λ = 0.6). Therefore, it can be expected that the PEG-solutions will have a considerably lower permeate flux at the higher concentrations.

The additional pressure drop shown in Figure 5.16 can be taken into account if the permeability of the membrane is corrected by:

$$B(C_{PEG}) = \frac{B}{1 + K_B x_{PEG}} \tag{5.29}$$

Here K_B is a correction factor for the membrane permeability.

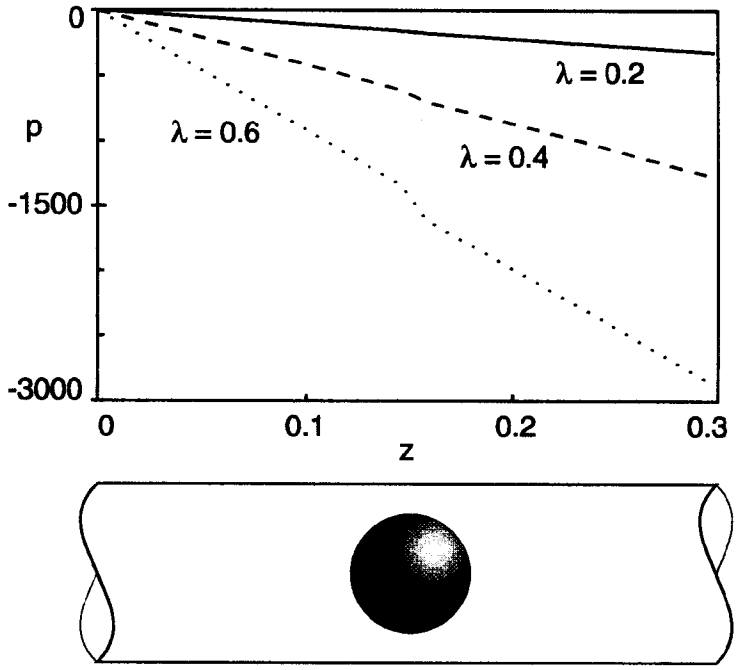

Figure 5.16 : The pressure drop in a tube filled with a spherical particle.

The only parameters that have to be estimated from the experimental data are the geometrical parameters of the membrane, the charge concentration of the membrane and the constant of equation 5.12.

Parameters from the clean water experiments

The clean water data are not sufficient to separately determine any of the parameters in our model. The flux of water alone is given by a simplified form of equation 5.11:

$$v_1 = -\left(\frac{D_{1,6} v_1}{RT} + \frac{d_p^2 \varepsilon}{32 \eta \tau^2} \right) \nabla p \qquad (5.30)$$

(The viscous flow term on the right is usually the most important). Fitting the measurements to this equation yields:

$$\frac{d_p^2 \varepsilon}{\tau^2} = 4.45 * 10^{-18} \qquad (5.31)$$

Parameters from the Water/PEG-4000 system

In total four parameters are estimated on the basis of the water/PEG-4000 experiments: the boundary layer constant (equation 5.12), the ratio ε/τ^2, the pore size and a permeability correction factor of the membrane.

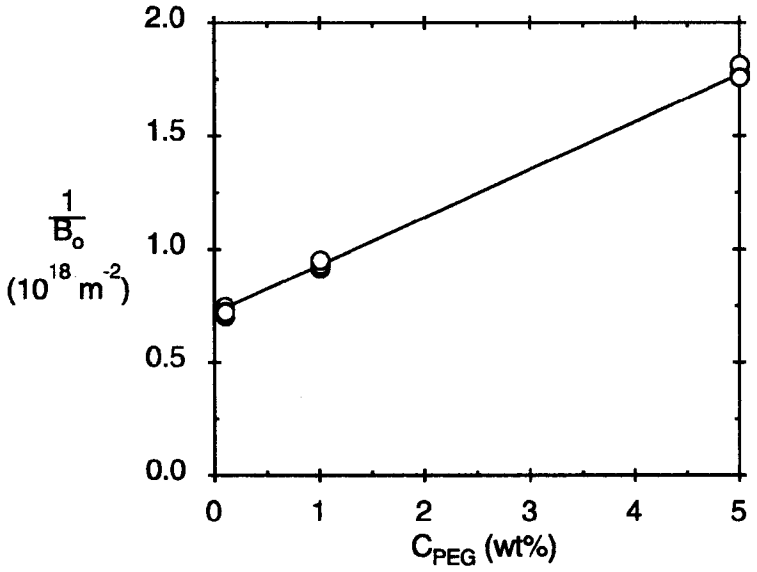

Figure 5.17: The inverse of the permeability as a function of the feed concentration.

Relation 5.31 was used as a constraint in the fitting of these experiments. Figure 5.17 gives the initial estimate of the membrane

permeability, which justifies the shape of equation 5.29. Table 5.2 gives the results of the estimated parameters. The results of the model are given in Figure 5.7. The tortuosity and porosity cannot be determined separately. However, the tortuosity would be expected to be in the range of 1.5 to 2 which yields porosities is the range of 0.08 to 0.14.

parameter	value
Const	0.5584
K_B	6331
ε/τ^2	0.0347
d_p	11.35 nm

Table 5.2: The parameters of the water/PEG-4000 system.

The water/potassium phosphate system

The only parameter estimated with the data of this system is the charge concentration of the membrane. The porosity was set to 0.1. The estimated charge concentration of the membrane was 2.0 mol/m^3. The calculated rejection of this system is shown in Figure 5.9.

The water/PEG-4000/potassium phosphate system

With the parameters from the two-solute experiments, we can describe the three-solute experiments. The results of the model are given in Figure 5.11 (rejections) and 5.12 (fluxes). The model rejection of PEG-4000 in the mixed systems is somewhat lower than the experimental results. The model rejection of potassium phosphate is also slightly different from the experimental results. Especially the rejection in the 5 mM phosphate/5 wt% PEG system is shifted to the left. The same effect is seen in the fluxes. The negative rejection of phosphate, found experimentally in the 50 mM phosphate/5 wt% PEG system, is predicted by the model.

Conclusions

The Maxwell-Stefan equation for diffusion has been used to develop a model to describe the performance of a single ultrafiltration stage. The

model has been tested with ultrafiltration experiments on PEG-4000 and potassium phosphate. From the experiments the pore size, the ratio ε/τ^2, and the charge concentration of the membrane are estimated. The orders of magnitude of these parameters are as expected. The model gave an accurate description of the single solute ultrafiltration of PEG-4000 and potassium phosphate. The mixed solute experiment are not described as accurately as the single solute experiments. However, the negative rejections found experimentally for phosphate in some measurements are predicted by the model.